Title

A low communication rate distributed inertial navigation architecture with cellular signal aiding

Authors

Morales, J.
Kassas, Z.

Publication Date

2018-06-01

Peer reviewed

A Low Communication Rate Distributed Inertial Navigation Architecture with Cellular Signal Aiding

Joshua Morales and Zaher M. Kassas
Department of Electrical and Computer Engineering
University of California, Riverside, USA
Emails: josmorales@engr.ucr.edu and zkassas@ieee.org

***Abstract*—A distributed, low communication rate architecture is proposed for collaborating vehicles to aid their inertial navigation systems (INSs) with cellular signals. The proposed approach compresses the amount of communicated data between vehicles by invoking mild approximations that reduce the communication rate by 91.7% from an optimal centralized approach, with a negligible impact on performance. Simulation and experimental results are presented demonstrating multiple unmanned aerial vehicles (UAVs) navigating via the proposed framework, aiding their INSs with cellular pseudoranges in the absence of GPS.**

I. Introduction

Modern vehicles integrate an inertial navigation system (INS) and a global navigation satellite system (GNSS) receiver. This integration benefits from complementary properties: the long-term stability of a GNSS navigation solution and the short term accuracy of an INS. However, it is known that in the inevitable event that GNSS signals become unusable (e.g., in deep urban canyons or in the presence of interference or jamming), a vehicle must rely entirely on its INS, in which case the errors of the navigation solution will quickly diverge. Recently, the exploitation of cellular signals has been demonstrated as an attractive alternative for navigation when GNSS signals become unusable [1], [2]. Cellular signals are attractive for aiding a vehicle's INS since their signals are: received at a high power, transmitted at high bandwidths, and are geographically abundant and geometrically diverse.

Collaboration is known to improve the navigation performance [3]. Collaborating vehicles making either inter-vehicle Doppler shift measurements [4] or range measurements [5] in the absence of GNSS have been shown to decrease the error divergence rate of their navigation solutions compared to a standalone INS. Instead of inter-vehicle measurements, collaborating vehicles may exchange measurements they make on terrestrial signals of opportunity, such as cellular signals [6]. In [7], multiple vehicles sharing INS information and cellular pseudoranges through a centralized framework was shown to bound INS errors in the absence of GNSS signals. Communicating INS information among vehicles comes with a large communication cost due to the substantial amount of INS data produced by each vehicle and the need to maintain inter-vehicle correlations. In [8], a distributed framework was presented that maintained inter-vehicle correlations for multiple vehicles aiding their INSs with cellular pseudoranges. However, the high communication cost was not addressed. This paper focuses on reducing the communication cost of a distributed cellular-aided INS.

This paper makes three contributions. First, the communication rate requirement of a distributed cellular-aided INS is compared to a full centralized approach. Second, a method to reduce the communication rate by 91.7% is presented, which approximates the INS data that needs to be transmitted. Third, the accuracy of the invoked approximation is studied by varying the reliability of the communication channel in terms of probability of packet drop. Experimental results are presented demonstrating two unmanned aerial vehicles (UAVs) aiding their INSs with the proposed distributed cellular-aided INS.

The remainder of the paper is organized as follows. Section II presents the dynamics and measurement models. Section III discusses the distributed cellular-aided INS. Section IV discusses a method to reduce communication rate. Section V demonstrates the performance of the distributed cellular-aided INS using the communication rate reduction method. Section VI provides experimental results. Concluding remarks are given in Section VII.

II. Model Description

A. Cellular Transmitter Dynamics Model

Each cellular signal is assumed to emanate from a spatially-stationary terrestrial transmitter. Its state vector will consist of three-dimensional (3-D) position states $\boldsymbol{r}_{\mathrm{s}_m} \triangleq [x_{\mathrm{s}_m}, y_{\mathrm{s}_m}, z_{\mathrm{s}_m}]^{\mathsf{T}}$ and clock error states $\boldsymbol{x}_{\mathrm{clk},\mathrm{s}_m} \triangleq \left[c\delta t_{\mathrm{s}_m}, c\dot{\delta} t_{\mathrm{s}_m}\right]^{\mathsf{T}}$, where c is the speed of light, δt_{s_m} is the clock bias, $\dot{\delta} t_{\mathrm{s}_m}$ is the clock drift, $m = 1, \ldots, M$, and M is the total number of transmitters.

The transmitters' discretized dynamics are given by

$$\boldsymbol{x}_{\mathrm{s}_m}(k+1) = \mathbf{F}_{\mathrm{s}}\, \boldsymbol{x}_{\mathrm{s}_m}(k) + \boldsymbol{w}_{\mathrm{s}_m}(k), \quad k = 1, 2, \ldots, \tag{1}$$

$$\boldsymbol{x}_{\mathrm{s}_m} = \left[\boldsymbol{r}_{\mathrm{s}_m}^{\mathsf{T}}, \boldsymbol{x}_{\mathrm{clk},\mathrm{s}_m}^{\mathsf{T}}\right]^{\mathsf{T}},$$

$$\mathbf{F}_{\mathrm{s}} = \mathrm{diag}\left[\mathbf{I}_{3\times 3}, \mathbf{F}_{\mathrm{clk}}\right], \quad \mathbf{F}_{\mathrm{clk}} = \begin{bmatrix} 1 & T \\ 0 & 1 \end{bmatrix},$$

where $\boldsymbol{w}_{\mathrm{s}_m}$ is the process noise, which is modeled as a discrete-time (DT) white noise sequence with covariance $\mathbf{Q}_{\mathrm{s}_m} = \mathrm{diag}\left[\mathbf{0}_{3\times 3}, c^2\mathbf{Q}_{\mathrm{clk},\mathrm{s}_m}\right]$, where

$$\mathbf{Q}_{\mathrm{clk},\mathrm{s}_m} = \begin{bmatrix} S_{w_{\delta t_{\mathrm{s},m}}} T + S_{w_{\dot{\delta} t_{\mathrm{s},m}}} \frac{T^3}{3} & S_{w_{\dot{\delta} t_{\mathrm{s},m}}} \frac{T^2}{2} \\ S_{w_{\dot{\delta} t_{\mathrm{s},m}}} \frac{T^2}{2} & S_{w_{\dot{\delta} t_{\mathrm{s},m}}} T \end{bmatrix}$$

and T is the constant sampling interval. The terms $S_{w_{\delta t_{\mathrm{s},m}}}$ and $S_{w_{\dot{\delta} t_{\mathrm{s},m}}}$ are the clock bias and drift process noise power spectra, respectively, which can be related to the power-law coefficients, $\{h_{\alpha,\mathrm{s}_m}\}_{\alpha=-2}^{2}$, which have been shown through laboratory experiments to characterize the power spectral density of the fractional frequency deviation of an oscillator from nominal frequency according to $S_{w_{\delta t_{\mathrm{s},m}}} \approx \frac{h_{0,\mathrm{s}_m}}{2}$ and $S_{w_{\dot{\delta} t_{\mathrm{s},m}}} \approx 2\pi^2 h_{-2,\mathrm{s}_m}$ [9].

B. Vehicle Dynamics Model

The state vector of each vehicle will consist of its INS state $\boldsymbol{x}_{B_n}$ and the receiver's clock error states $\boldsymbol{x}_{\mathrm{clk},r_n} \triangleq \left[c\delta t_{r_n},\, c\dot{\delta} t_{r_n}\right]^{\mathsf{T}}$, i.e., $\boldsymbol{x}_{r_n} = \left[\boldsymbol{x}_{B_n}^{\mathsf{T}},\, \boldsymbol{x}_{\mathrm{clk},r_n}^{\mathsf{T}}\right]^{\mathsf{T}}$, where $n = 1,\ldots,N$, and N is the total number of vehicles.

The INS 16-state vector is

$$\boldsymbol{x}_{B_n} = \left[{}^{B}_{G}\bar{\boldsymbol{q}}_n^{\mathsf{T}},\quad \boldsymbol{r}_{r_n}^{\mathsf{T}},\quad \boldsymbol{v}_{r_n}^{\mathsf{T}},\quad \boldsymbol{b}_{g_n}^{\mathsf{T}},\quad \boldsymbol{b}_{a_n}^{\mathsf{T}}\right]^{\mathsf{T}},$$

where ${}^{B}_{G}\bar{\boldsymbol{q}}_n$ is the 4-D unit quaternion in vector-scalar form, which represents the orientation of the body frame with respect to a global frame [10], e.g., the Earth-centered inertial frame; $\boldsymbol{r}_{r_n}$ and $\boldsymbol{v}_{r_n}$ are the 3-D position and velocity, respectively, of the vehicle's body frame expressed in a global frame; and $\boldsymbol{b}_{g_n}$ and $\boldsymbol{b}_{a_n}$ are the gyroscope and accelerometer biases, respectively.

1) Receiver Clock State Dynamics: The vehicle-mounted receiver's clock error states will evolve in time according to

$$\boldsymbol{x}_{\mathrm{clk},r_n}(k+1) = \mathbf{F}_{\mathrm{clk}}\boldsymbol{x}_{\mathrm{clk},r_n}(k) + \boldsymbol{w}_{\mathrm{clk},r_n}(k), \qquad (2)$$

where $\boldsymbol{w}_{\mathrm{clk},r_n}$ is the process noise vector, which is modeled as a DT white noise sequence with covariance $\mathbf{Q}_{\mathrm{clk},r_n}$, which has an identical form to $\mathbf{Q}_{\mathrm{clk},\mathrm{s}_m}$, except that $S_{w_{\delta t_{\mathrm{s},m}}}$ and $S_{w_{\dot{\delta} t_{\mathrm{s},m}}}$ are now replaced with receiver-specific spectra $S_{w_{\delta t_{r,n}}}$ and $S_{w_{\dot{\delta} t_{r,n}}}$, respectively.

2) INS State Kinematics: The INS states will evolve in time according to

$$\boldsymbol{x}_{B_n}(k+1) = \boldsymbol{f}_{B_n}\left[\,\boldsymbol{x}_{B_n}(k), {}^{B}\boldsymbol{\omega}_n(t_k), {}^{G}\boldsymbol{a}_n(t_k)\,\right],$$

where $\boldsymbol{f}_{B_n}$ is a vector-valued function of standard kinematic equations, which are driven by the 3-D rotational rate vector ${}^{B}\boldsymbol{\omega}_n$ in the body frame and the 3-D acceleration of the IMU ${}^{G}\boldsymbol{a}_n$ in the global frame [11].

3) IMU Measurement Model: The IMU on the n^{th} vehicle contains a triad-gyroscope and a triad-accelerometer, which produce measurements $\boldsymbol{z}_{\mathrm{imu}_n} \triangleq \left[\boldsymbol{\omega}_{\mathrm{imu}_n}^{\mathsf{T}},\, \boldsymbol{a}_{\mathrm{imu}_n}^{\mathsf{T}}\right]^{\mathsf{T}}$ of the angular rate and specific force, which are modeled as

$$\boldsymbol{\omega}_{\mathrm{imu}_n} = {}^{B}\boldsymbol{\omega}_n + \boldsymbol{b}_{g_n} + \boldsymbol{n}_{g_n} \qquad (3)$$

$$\boldsymbol{a}_{\mathrm{imu}_n} = \mathbf{R}\left[{}^{B_k}_{G}\bar{\boldsymbol{q}}_n\right]\left({}^{G}\boldsymbol{a}_n - {}^{G}\boldsymbol{g}_n\right) + \boldsymbol{b}_{a_n} + \boldsymbol{n}_{a_n}, \qquad (4)$$

where ${}^{B}\boldsymbol{\omega}_n$ is the 3-D rotational rate vector, ${}^{G}\boldsymbol{a}_n$ is the 3-D acceleration of the IMU in the global frame, ${}^{B_k}_{G}\bar{\boldsymbol{q}}_n$ represents the orientation of the body frame in a global frame at time-step k, $\mathbf{R}\left[\bar{\boldsymbol{q}}_n\right]$ is the equivalent rotation matrix of $\bar{\boldsymbol{q}}_n$, ${}^{G}\boldsymbol{g}_n$ is the acceleration due to gravity of the n^{th} vehicle in the global frame, and $\boldsymbol{n}_{g_n}$ and $\boldsymbol{n}_{a_n}$ are measurement noise vectors, which are modeled as white noise sequences with covariances $\sigma_{g_n}^2\,\mathbf{I}_{3\times 3}$ and $\sigma_{a_n}^2\,\mathbf{I}_{3\times 3}$, respectively.

C. Receiver Observation Model

The pseudorange observation made by the n^{th} receiver on the m^{th} cellular transmitter at time-step j, after discretization and mild approximations discussed in [12], is given by

$$z_{r_n,\mathrm{s}_m}(j) = \|\boldsymbol{r}_{r_n}(j) - \boldsymbol{r}_{\mathrm{s}_m}\|_2 + c\cdot\left[\delta t_{r_n}(j) - \delta t_{\mathrm{s}_m}(j)\right] + v_{r_n,\mathrm{s}_m}(j), \qquad (5)$$

where v_{r_n,s_m} is the measurement noise which is modeled as a DT zero-mean white Gaussian sequence with variance $\sigma_{r_n,\mathrm{s}_m}^2$. The pseudorange observation made by the n^{th} receiver on the l^{th} GNSS space vehicle (SV), after compensating for ionospheric and tropospheric delays is given by

$$z_{r_n,\mathrm{sv}_l}(j) = \|\boldsymbol{r}_{r_n}(j) - \boldsymbol{r}_{\mathrm{sv}_l}(j)\|_2 + c\cdot\left[\delta t_{r_n}(j) - \delta t_{\mathrm{sv}_l}(j)\right] + v_{r_n,\mathrm{sv}_l}(j), \qquad (6)$$

where $z_{r_n,\mathrm{sv}_l} \triangleq z'_{r_n,\mathrm{sv}_l} - c\delta t_{\mathrm{iono}} - c\delta t_{\mathrm{tropo}}$; δt_{iono} and $\delta t_{\mathrm{tropo}}$ are the ionospheric and tropospheric delays, respectively; z'_{r_n,sv_l} is the uncompensated pseudorange; v_{r_n,sv_l} is the measurement noise, which is modeled as a DT zero-mean white Gaussian sequence with variance $\sigma_{r_n,\mathrm{sv}_l}^2$; $l = 1,\ldots,L$; and L is the total number of GNSS SVs.

III. Distributed Cellular-Aided Inertial Navigation

In this section, the distributed cellular-aided INS framework depicted in Fig. 1 is described.

A. Framework Overview

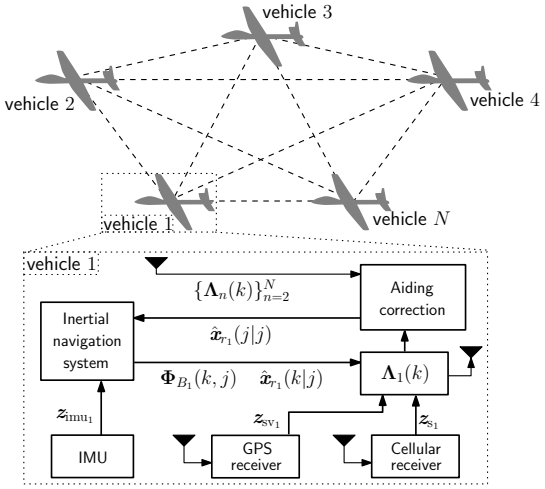

Fig. 1. Distributed cellular-aided INS framework. All N vehicles maintain their own INSs. When pseudoranges are available from GNSS satellites $\boldsymbol{z}_{\mathrm{sv}}$ or cellular transmitters $\boldsymbol{z}_{\mathrm{s}}$, each vehicle transmits a packet $\mathbf{\Lambda}_n(k)$ containing required information for each vehicle to produce an aiding correction.

This framework operates in two modes. In the first mode, both GNSS SV and cellular pseudoranges are available, i.e., the measurements are $\boldsymbol{z} \equiv \left[\boldsymbol{z}_{\mathrm{sv}}^{\mathsf{T}},\, \boldsymbol{z}_{\mathrm{s}}^{\mathsf{T}}\right]^{\mathsf{T}}$, where

$$\boldsymbol{z}_{\mathrm{sv}} \triangleq \left[\,\boldsymbol{z}_{r_1,\mathrm{sv}}^{\mathsf{T}},\ldots,\boldsymbol{z}_{r_N,\mathrm{sv}}^{\mathsf{T}}\,\right]^{\mathsf{T}},\ \boldsymbol{z}_{\mathrm{s}} \triangleq \left[\,\boldsymbol{z}_{r_1,\mathrm{s}}^{\mathsf{T}},\ldots,\boldsymbol{z}_{r_N,\mathrm{s}}^{\mathsf{T}}\,\right]^{\mathsf{T}},$$

$\boldsymbol{z}_{r_n,\mathrm{sv}} = [z_{r_n,\mathrm{sv}_1}, \ldots, z_{r_n,\mathrm{sv}_L}]^{\mathsf{T}}$, $\boldsymbol{z}_{r_n,\mathrm{s}} = [z_{r_n,\mathrm{s}_1}, \ldots, z_{r_n,\mathrm{s}_M}]^{\mathsf{T}}$.

These measurements are shared and fused through an extended Kalman filter (EKF) to improve the navigation solution compared to a standalone GNSS-aided INS. In the second mode, GNSS signals are unavailable and only cellular pseudoranges are available, i.e., $\boldsymbol{z} \equiv \boldsymbol{z}_{\mathrm{s}}$. These measurements are used exclusively to provide INS aiding corrections. It is assumed that the cellular transmitters positions are known from databases or from, *a priori* mapping [13]. However, their clock states are dynamic and stochastic; hence, they must be continuously estimated. Therefore, the EKF state vector consists of all vehicles' states and all transmitters' clock states, namely

$$\boldsymbol{x} \triangleq \left[\boldsymbol{x}_{r_1}^{\mathsf{T}}, \ldots, \boldsymbol{x}_{r_N}^{\mathsf{T}}, \boldsymbol{x}_{\mathrm{clk},\mathrm{s}_1}^{\mathsf{T}}, \ldots, \boldsymbol{x}_{\mathrm{clk},\mathrm{s}_M}^{\mathsf{T}}\right]^{\mathsf{T}}.$$

Each vehicle employs its own EKF to produce an estimate $\hat{\boldsymbol{x}}(k|j) \triangleq \mathbb{E}[\boldsymbol{x}(k)|\boldsymbol{Z}^j]$ of $\boldsymbol{x}(k)$ and an associated estimation error covariance $\mathbf{P}(k|j) \triangleq \mathbb{E}[\tilde{\boldsymbol{x}}(k|j)\tilde{\boldsymbol{x}}^{\mathsf{T}}(k|j)|\boldsymbol{Z}^j]$, where $\tilde{\boldsymbol{x}}$ is the estimation error, $\boldsymbol{Z}^j \triangleq \{\boldsymbol{z}(i)\}_{i=1}^{j}$, and $k \geq j$.

B. Distributed Aided-INS Filter Structure

Between aiding pseudoranges, each vehicle uses its own INS and the clock model (2) to propagate its own state $\hat{\boldsymbol{x}}_{r_n}$ and the corresponding linearized state transition matrix $\mathbf{F}_{r_n}(k,j) \triangleq \mathrm{diag}\left[\boldsymbol{\Phi}_{B_n}(k,j), \mathbf{F}_{\mathrm{clk}}^K\right]$, where $\boldsymbol{\Phi}_{B_n}$ is the DT linearized INS state transition matrix of the n^{th} vehicle, which is constructed from IMU data $\boldsymbol{z}_{\mathrm{imu}_n}$ from t_j to t_k. When aiding pseudoranges become available, each vehicle computes a centralized equivalent prediction and update. The prediction is given by

$$\mathbf{P}(k|j) = \mathbf{F}(k,j)\mathbf{P}(j|j)\mathbf{F}^{\mathsf{T}}(k,j) + \mathbf{Q}(k,j), \tag{7}$$

where iteration j is the last time a set of aiding pseudoranges were available, iteration k is the current iteration, $\mathbf{Q}$ is the process noise covariance, and

$$\mathbf{F}(k,j) \triangleq \mathrm{diag}\left[\mathbf{F}_{r_1}(k,j), \ldots, \mathbf{F}_{r_N}(k,j), \mathbf{F}_{\mathrm{s}}^K, \ldots, \mathbf{F}_{\mathrm{s}}^K\right].$$

The structures of $\boldsymbol{\Phi}_{B_n}$ and $\mathbf{Q}$ are described in [8]. Note that $\mathbf{F}$ can not be readily constructed at each vehicle, since it depends on IMU data from all collaborating vehicles. IMU data-rates are typically between 100 Hz and 400 Hz, making the transmission of IMU data from all collaborating vehicles undesirable. Therefore, instead of transmitting IMU data, each vehicle broadcasts a packet $\boldsymbol{\Lambda}_n$ only when aiding pseudoranges become available, which typically occur between 1 Hz and 5 Hz, and is given by

$$\boldsymbol{\Lambda}_n(k) \triangleq \{\hat{\boldsymbol{x}}_{B_n}(k|j), \boldsymbol{\Phi}_{B_n}(k,j), \boldsymbol{z}_{r_n,\mathrm{sv}}(k), \boldsymbol{z}_{r_n,\mathrm{s}}(k)\}. \tag{8}$$

Assuming a fully-connected graph, i.e., all vehicles can send and receive packets as depicted in Fig. 1, each vehicle may then perform the centralized-equivalent update, given by

$$\begin{aligned} \hat{\boldsymbol{x}}(k|k) &= \hat{\boldsymbol{x}}(k|j) + \mathbf{K}(k)\left[\boldsymbol{z}(k) - \hat{\boldsymbol{z}}(k)\right] \\ \mathbf{P}(k|k) &= \mathbf{P}(k|j) - \mathbf{K}(k)\mathbf{H}(k)\mathbf{P}(k|j), \end{aligned} \tag{9}$$

where $\mathbf{K}$ is the Kalman gain matrix, $\hat{\boldsymbol{z}}$ is the predicted measurement, and $\mathbf{H}$ is the measurement Jacobian evaluated at the state prediction $\hat{\boldsymbol{x}}(k|j)$. The structures of these matrices are described in detail in [7], [8].

While the packet (8) is transmitted at a lower frequency compared to IMU data, the transmission of $\boldsymbol{\Phi}_{B_n}$ in (8) still requires a large communication bit-rate, since it is a 15×15 matrix, requiring the transmission of 225 values every update. This communication burden is addressed in the next section.

IV. Communication Rate Reduction

The number of elements that must be transmitted to communicate $\boldsymbol{\Phi}_{B_n}$ to each vehicle can be reduced from 225 to 32 by exploiting the structure of $\boldsymbol{\Phi}_{B_n}$ and invoking some mild approximations. Each vehicle can then reconstruct an approximation of $\boldsymbol{\Phi}_{B_n}$ using the received 32 elements with only a minimal impact on performance.

The structure of $\boldsymbol{\Phi}_{B_n}$ after a K-step propagation can be shown to be approximately

$$\boldsymbol{\Phi}_{B_n}(k,j) \approx \begin{bmatrix} \mathbf{I}_3 & \mathbf{0}_3 & \mathbf{0}_3 & KT\mathbf{R}[\boldsymbol{q}_{n,1}] & \mathbf{0}_3 \\ \lfloor \boldsymbol{v}_n \times \rfloor & \mathbf{I}_3 & \mathbf{I}_3 T & \mathbf{A}_n & \frac{KT^2}{2}\mathbf{R}[\boldsymbol{q}_{n,2}] \\ \lfloor \boldsymbol{y}_n \times \rfloor & \mathbf{0}_3 & \mathbf{I}_3 & \mathbf{B}_n & KT\mathbf{R}[\boldsymbol{q}_{n,1}] \\ \mathbf{0}_3 & \mathbf{0}_3 & \mathbf{0}_3 & \mathbf{I}_3 & \mathbf{0}_3 \\ \mathbf{0}_3 & \mathbf{0}_3 & \mathbf{0}_3 & \mathbf{0}_3 & \mathbf{I}_3 \end{bmatrix}, \tag{10}$$

where $K = k - j$; $\lfloor \boldsymbol{v}_n \times \rfloor$ and $\lfloor \boldsymbol{y}_n \times \rfloor$ are skew symmetric matrices whose elements are defined from the vectors $\boldsymbol{v}_n$ and $\boldsymbol{y}_n$, respectively; the vectors $\boldsymbol{q}_{n,1}$ and $\boldsymbol{q}_{n,2}$ are quaternions; and $\mathbf{A}_n$ and $\mathbf{B}_n$ are arbitrarily structured 3×3 matrices. Note the following two properties of the structure (10). First, since $\boldsymbol{v}_n$ and $\boldsymbol{y}_n$ maintain a skew symmetric form, they can be transmitted using only three elements each. Second, since the scaling pre-multiplying the matrices $\mathbf{R}[\boldsymbol{q}_{n,1}]$ and $\mathbf{R}[\boldsymbol{q}_{n,2}]$ is deterministic and only dependent on the IMU sampling period T and the number of iterations K, these matrices can be converted to quaternions $\boldsymbol{q}_{n,1}$ and $\boldsymbol{q}_{n,2}$, transmitted using only four elements each, and then be re-assembled at each corresponding vehicle. Therefore, if each vehicle replaces $\boldsymbol{\Phi}_{B_n}(k,j)$ with $\{\boldsymbol{v}_n, \boldsymbol{y}_n, \boldsymbol{q}_{n,1}, \boldsymbol{q}_{n,2}, \mathbf{A}_n, \mathbf{B}_n\}$ in (8), only 32 elements need to be transmitted instead of 225.

Next, the communication rate requirements of the approximation (10) is compared against the requirements of a full centralized approach. The data that must be communicated to support the centralized approach and the distributed approach with the approximation (10) along with their corresponding data-rate requirements are tabulated in Table I and Table II, respectively.

The required data-rate of the centralized approach r_{cent} is found by summing the entries of the right column of Table I and multiplying by the number of collaborating vehicles and the number of bits representing the data type b, yields

$$r_{\mathrm{cent}} = bN \cdot \left[6f_{\mathrm{imu}} + (2M + 16)f_{\mathrm{s}}\right].$$

Setting the IMU data-rate to $f_{\mathrm{imu}} \equiv 100\mathrm{Hz}$, the cellular pseudorange data-rate to $f_{\mathrm{s}} \equiv 1\mathrm{Hz}$, the number of cellular transmitter to $M \equiv 6$, and assuming each value is a 32 bit float data type, the required bit-rate is $N \cdot (20.096)\,\mathrm{kbits/sec}$.

TABLE I
REQUIRED DATA-RATE: CENTRALIZED

Data Type	Data-Rate (values@rate)
Accelerometer ($\boldsymbol{a}_{\text{imu}_n}$)	$3\,@f_{\text{imu}}$
Gyroscope ($\boldsymbol{\omega}_{\text{imu}_n}$)	$3\,@f_{\text{imu}}$
Cellular pseudoranges (z_{r_n,s_m})	$M-1\,@f_{\text{s}}$
pseudorange uncertainty ($\mathbf{R}$)	$M-1\,@f_{\text{s}}$
State update ($\hat{\boldsymbol{x}}_{r_n}$)	$18@f_{\text{s}}$

TABLE II
REQUIRED DATA-RATE: DISTRIBUTED

Data Type	Data-Rate (values@rate)
Position ($\hat{\boldsymbol{r}}_{r_n}$)	$3\,@f_{\text{s}}$
Velocity ($\hat{\boldsymbol{v}}_{r_n}$)	$3\,@f_{\text{s}}$
Orientation ($\hat{\boldsymbol{q}}_n$)	$4\,@f_{\text{s}}$
Cellular pseudoranges (z_{r_n,s_m})	$M-1\,@f_{\text{s}}$
pseudorange uncertainty ($\mathbf{R}$)	$M-1\,@f_{\text{s}}$
$\{\boldsymbol{v}_n, \boldsymbol{y}_n, \boldsymbol{q}_{n,1}, \boldsymbol{q}_{n,2}, \mathbf{A}_n, \mathbf{B}_n\}$	$32\,@f_{\text{s}}$

Similarly, the required data-rate of the distributed approach r_{dist} using the approximation can be found from Table II to be given by

$$r_{\text{dist}} = bN \cdot (2M + 40)\, f_{\text{s}}.$$

Using the same previous settings for f_{imu}, f_{s}, and M, the required bit-rate is $N \cdot (1.664)\,\text{kbits/sec}$, a 91.7% bit-rate reduction.

Although the approximation (10) significantly reduces the required bit-rate, the accuracy of the approximation is dependent on the time between INS aiding updates and the vehicles' maneuvers. Furthermore, the transmission of the packets $\boldsymbol{\Lambda}_n(k)$ may fail, in which case the time between aiding updates further increases, which degrades the approximation. The next section studies the robustness of the approximation in a lossy communication channel.

V. PERFORMANCE CHARACTERIZATION

In this section, the robustness of the approximation (10) is studied when the framework is subject to random drops of the data packets $\{\boldsymbol{\Lambda}_n(k)\}_{n=1}^{N}$.

A. Probability of Packet Drop

The vehicles are assumed to communicate in a channel with Bernoulli packet dropouts. This modifies the measurement update (9) to take the form

$$\begin{cases} \hat{\boldsymbol{x}}(k|k) = \hat{\boldsymbol{x}}(k|j), & \gamma(k) = 0 \\ \mathbf{P}(k|k) = \mathbf{P}(k|j); & \\ \hat{\boldsymbol{x}}(k|k) = \hat{\boldsymbol{x}}(k|j) + \mathbf{K}(k)\left[\boldsymbol{z}(k) - \hat{\boldsymbol{z}}(k)\right], & \gamma(k) = 1 \\ \mathbf{P}(k|k) = \mathbf{P}(k|j) - \mathbf{K}(k)\mathbf{H}(k)\mathbf{P}(k|j); & \end{cases}$$

where $\gamma(k) \sim \mathcal{B}(1-p)$, i.e., a Bernoulli random sequence with probability of failure p [14]. The value of p depends on the environment and the communication protocol employed. In this work, the vehicles are assumed to employ the Dedicated Short Range Communication (DSRC) technology, which is an IEEE 802.11p wireless standard supported by the U.S. Department of Transportation to enable future vehicle-to-vehicle and vehicle-to-infrastructure communications. The Federal Communications Commission allocates 75 MHz of spectrum in the 5.9 GHz frequency band. The signal characteristics of DSRC in real-world automobile settings are well studied and are expected to support $6\,\text{Mbits/sec}$ when the received power is greater than $-95\,\text{dBm}$ [15].

To determine realistic values of p for UAVs, a study was conducted using Wireless InSite®, a signal propagation simulator developed by Remcom. Detailed 3-D City model files were imported from the website of the city of Portland, Oregon [16] and two UAV trajectories (UAV a and UAV b) were generated at an altitude just below the height of the tallest buildings. The path loss of signals propagating from three points on UAV b's trajectory to all points sampled with 10 meter spacing on UAV a's trajectory were calculated. A screen shot of the ray tracing used to simulate the signal propagation is provided in Fig. 2. The resulting cumulative distribution function (CDF) curve of the path loss corresponding to each of the three points from UAV b's trajectory are illustrated in Fig. 3.

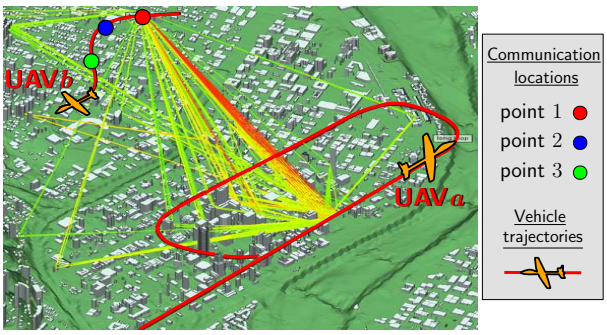

Fig. 2. Communication path loss study for two UAVs in Portland, Oregon. The trajectory of UAV a was sampled with 10 meter spacing. Three separate points (red, blue, and green dots) were sampled along the trajectory of UAV b. For each of these three points, the path loss (dB) was calculated to each of the sampled points along the trajectory of UAV a. Only ray tracing from the red point of UAV b to a small number of points along the trajectory of UAV a are shown to avoid cluttering the figure.

Using the properties of the DSRC and under typical transmit and received powers and antenna gains, it can be shown that 115 dB is the tolerable path loss before packet dropouts begin to occur. Note from the CDF in Fig. 3 that the probability $1-p$ of being under the tolerable path loss 115 dB lies in the range $(0.3, 0.55)$. Therefore, realistic values for p in this particular scenario are between $(0.45, 0.7)$.

B. Robustness Analysis

In this section, the robustness of the approximation (10) is studied through Monte Carlo analysis. To this end, the trajectories of $N = 3$ UAVs were simulated in the vicinity of $M = 6$ cellular transmitters as depicted in Fig. 4(a).

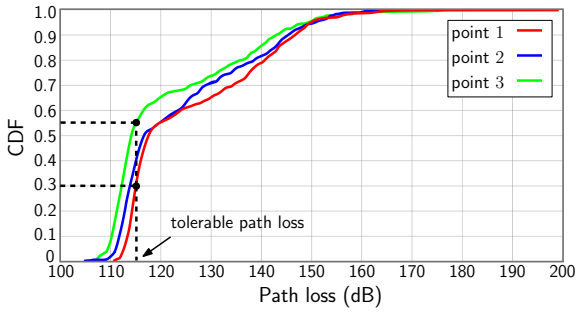

Fig. 3. Resulting CDF curve of the path loss (dB) for signals propagating from points 1,2, and 3 to points sampled on UAV a's trajectory, as illustrated in Fig. 2.

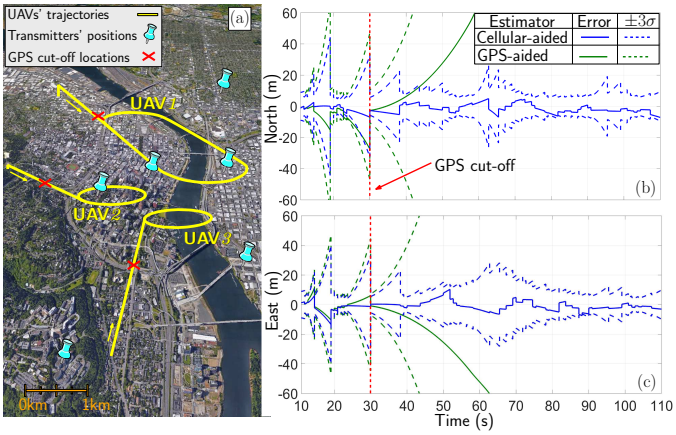

Fig. 4. (a) UAV trajectories and cellular transmitter locations. (b) UAV 1 north position errors and $\pm 3\sigma$ bounds. (c) UAV 1 east position errors and $\pm 3\sigma$ bounds.

The UAVs' trajectories were generated using a six degree of freedom model for quad-rotors. Consumer grade gyroscope and accelerometer data was simulated according to (3) and (4), respectively. Cellular transmitter pseudoranges were generated at 1 Hz using (5) and (1), with $\{h_{0,\mathrm{s}_m}, h_{-2,\mathrm{s}_m}\}_{m=1}^{6} \equiv \{8 \times 10^{-20}, 4 \times 10^{-23}\}$, which correspond to a typical oven-controlled crystal oscillator (OCXO). GPS L1 C/A pseudoranges were generated at 1 Hz according to (6) using SV orbits produced from Receiver Independent Exchange (RINEX) files downloaded on May 31, 2017, and the clock model (2), with $\{h_{0,r_n}, h_{-2,r_n}\}_{n=1}^{3} = \{9.4 \times 10^{-20}, 3.8 \times 10^{-21}\}$, which correspond to a typical temperature-compensated crystal oscillator (TCXO). The GPS pseudoranges were set to be available for the first 30 seconds of the 110 second simulation.

First, single run results using $p \equiv 0.5$ are shown to demonstrate the performance of the distributed cellular-aided INS using the approximation (10). Two estimators were employed to estimate the UAVs' trajectories: (i) the distributed cellular-aided INS with the proposed approximation (10) and (ii) for a comparative analysis, a traditional GPS-aided INS. The resulting north and east position errors and corresponding $\pm 3\sigma$ bounds for UAV 1 are plotted in Fig. 4(b)–(c), respectively. Note from these plots, that even with a high probability of loss $p = 0.5$, the errors associated with distributed cellular-aided INS are bounded after GPS becomes unavailable at 30 seconds, whereas the errors associated with a traditional GPS-aided INS begin to diverge.

Next, 500 Monte Carlo runs were conducted for each value of $p \in \{0, 0.3, 0.6, 0.9\}$. For each run, two distributed cellular-aiding architectures were employed: (1) with the approximation and (2) without the approximation. Define the error $\tilde{\xi}_n$ introduced into the position estimate of vehicle n due to the approximation as

$$\tilde{\xi}_n(k|j) \triangleq \|\hat{\boldsymbol{r}}_{r_n}(k|j) - \hat{\boldsymbol{r}}'_{r_n}(k|j)\|, \tag{11}$$

where $\hat{\boldsymbol{r}}_{r_n}$ and $\hat{\boldsymbol{r}}'_{r_n}$ are the position estimates of vehicle n without and with the approximation, respectively. The root-mean squared (RMS) error with $\kappa = 500$ Monte Carlo runs is calculated as

$$\mathrm{RMS}\left[\tilde{\xi}_n(k|j)\right] = \sqrt{\frac{1}{\kappa}\sum_{i=1}^{\kappa} {}^{i}\tilde{\xi}^2_{r_n}(k|j)},$$

where ${}^{i}\tilde{\xi}_n(k|j)$ is the approximation error in the i^{th} run. This is plotted in Fig. 5 for UAV 1. It can be seen from Fig. 5 that for 80 seconds of GPS unavailability, the approximation-induced error introduced into the position estimate of UAV 1 remained less than 1m for a probability of packet drop as high as $p = 0.6$.

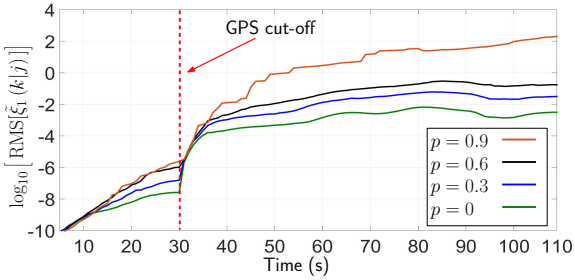

Fig. 5. RMS error results for the approximation error (11) for UAV 1 from Fig. 4 (a). For each value of $p \in \{0, 0.3, 0.6, 0.9\}$, 500 Monte Carlo runs were conducted to produce the corresponding $\mathrm{RMS}\left[\tilde{\xi}_1(k|j)\right]$ trajectory.

VI. Experimental Results

An experiment using two UAVs was conducted in Riverside, California to demonstrate the performance of the distributed cellular-aided INS framework using the communication rate reduction method described in Section IV. Each UAV was equipped with an Ettus® E312 universal software radio peripheral (USRP) to record both GPS and cellular signals. These USRPS were tuned to 1575.42 MHz to sample GPS L1 C/A signals and 882.75 MHz to sample Verizon cellular base transceiver stations (BTSs) whose signals were modulated through code division multiple access (CDMA). The in-phase and quadrature components of these signals were fed to the Multichannel Adaptive TRansceiver Information eXtractor (MATRIX) software-defined radio, which produced pseudorange observables to ten GPS SVs and two cellular BTSs [17] [18]. The IMU data was recorded from each UAV's on-board proprietary navigation system, which was developed by Autel Robotics®.

The UAVs were flown for 90 seconds in the vicinity of the two BTSs as illustrated in Figs. 6(a). Two estimators were implemented to estimate the flown trajectories: (i) the distributed cellular-aided INS described in Section III, and for a comparative analysis (ii) a traditional GPS-aided INS. To evaluate the accuracy of the approximation invoked to reduce the required communication bit-rate, the communication of the packets (8) were simulated to experience packet drops with a probability $p = 0$ and $p = 0.3$.

GPS was available for only the first 75 seconds of the run. The final north-east errors of the traditional GPS-aided INSs' navigation solutions after GPS became unavailable were 27.8 and 24.5 meters, respectively. The final errors of the UAVs' trajectories for the cellular-aided INS ($p = 0$) were 3.9 and 4.1 meters, respectively, and the final error (11) introduced by the approximation was a negligible $\tilde{\xi}_1 = 4.2 \times 10^{-2}$ and $\tilde{\xi}_2 = 4.9 \times 10^{-2}$ meters, respectively. The final errors of the UAVs' trajectories for the cellular-aided INS ($p = 0.3$) were 8.4 and 4.3 meters, respectively, and the final errors introduced by the approximation were $\tilde{\xi}_1 = 5.8 \times 10^{-2}$ and $\tilde{\xi}_2 = 6.3 \times 10^{-2}$ meters, respectively. While the cellular-aided INS errors are significantly less than the INS-only errors, an even greater reduction is expected when more cellular transmitters are used.

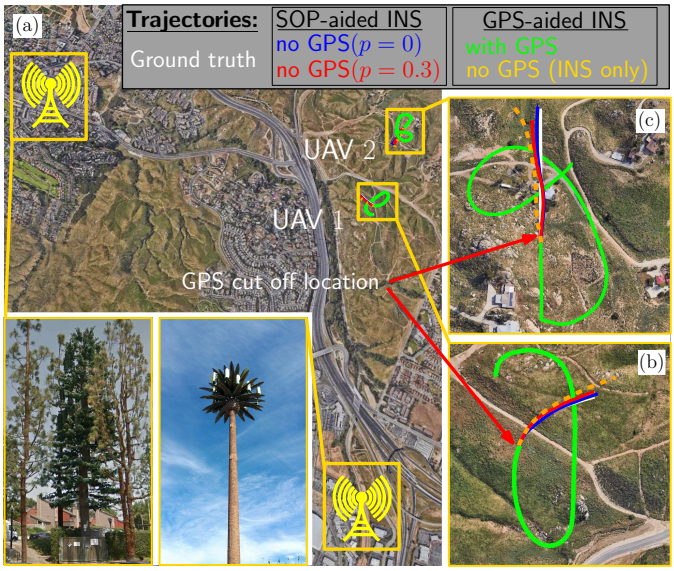

Fig. 6. Experimental results. (a) Cellular transmitter locations. (b) UAV 1 trajectory and estimates. (c) UAV 2 trajectory and estimates.

VII. Conclusions

A low communication rate distributed INS architecture with cellular aiding was presented. The communication rate was shown to be reduced by 91.7% from a full centralized approach. The robustness of the proposed framework was studied in a lossy channel with Bernoulli packet dropouts, and it was demonstrated through Monte Carlo analysis that the error due to the proposed approximation was minimal. Experimental results demonstrated a negligible impact on performance due to invoking the proposed communication rate reduction approach.

Acknowledgment

This work was supported in part by the Office of Naval Research (ONR) under Grant N00014-16-1-2305 and in part by the National Science Foundation (NSF) under Grant 1566240. This work was also supported in part by a grant from the National Center for Sustainable Transportation (NCST), supported by the U.S. Department of Transportation (USDOT).

References

[1] C. Yang, T. Nguyen, and E. Blasch, "Mobile positioning via fusion of mixed signals of opportunity," *IEEE Aerospace and Electronic Systems Magazine*, vol. 29, no. 4, pp. 34–46, April 2014.

[2] Z. Kassas, J. Khalife, K. Shamaei, and J. Morales, "I hear, therefore I know where I am: Compensating for GNSS deficiencies with cellular signals." *IEEE Signal Processing Magazine*, pp. 111–124, September 2017.

[3] C. Yang and A. Soloviev, "Covariance analysis of spatial and temporal effects of collaborative navigation," *NAVIGATION, Journal of the Institute of Navigation*, vol. 61, no. 3, pp. 213–225, 2014.

[4] N. Alam, A. Kealy, and A. Dempster, "Cooperative inertial navigation for GNSS-challenged vehicular environments," *IEEE Transactions on Intelligent Transportation Systems*, vol. 14, no. 3, pp. 1370–1379, September 2013.

[5] H. Mokhtarzadeh and D. Gebre-Egziabher, "Cooperative inertial navigation," *NAVIGATION, Journal of the Institute of Navigation*, vol. 61, no. 2, pp. 77–94, 2014.

[6] Z. Kassas, "Analysis and synthesis of collaborative opportunistic navigation systems," Ph.D. dissertation, The University of Texas at Austin, USA, 2014.

[7] J. Morales, J. Khalife, and Z. Kassas, "Collaborative autonomous vehicles with signals of opportunity aided inertial navigation systems," in *Proceedings of ION International Technical Meeting Conference*, January 2017, 805–818.

[8] J. Morales and Z. Kassas, "Distributed signals of opportunity aided inertial navigation with intermittent communication," in *Proceedings of ION GNSS Conference*, September 2017, pp. 2519–2530.

[9] A. Thompson, J. Moran, and G. Swenson, *Interferometry and Synthesis in Radio Astronomy*, 2nd ed. John Wiley & Sons, 2001.

[10] M. Shuster, "A survey of attitude representations," *The Journal of the Astronautical Sciences*, vol. 41, no. 4, pp. 439–517, October 1993.

[11] J. Farrell and M. Barth, *The Global Positioning System and Inertial Navigation*. New York: McGraw-Hill, 1998.

[12] Z. Kassas and T. Humphreys, "Observability analysis of collaborative opportunistic navigation with pseudorange measurements," *IEEE Transactions on Intelligent Transportation Systems*, vol. 15, no. 1, pp. 260–273, February 2014.

[13] J. Morales and Z. Kassas, "Optimal collaborative mapping of terrestrial transmitters: receiver placement and performance characterization," *IEEE Transactions on Aerospace and Electronic Systems*, 2016, accepted.

[14] X. Liu, L. Li, Z. Li, T. Fernando, and H. Iu, "Stochastic stability condition for the extended Kalman filter with intermitent observations," *IEEE Transactions on Circuits and Systems*, vol. 64, no. 3, pp. 334–338, March 2017.

[15] L. Cheng, B. Henty, D. Stancil, F. Bai, and P. Mudalige, "Mobile vehicle-to-vehicle narrow-band channel measurement and characterization of the 5.9 GHz dedicated short range communication (DSRC) frequency band," *IEEE Journal on Selected Areas in Communications*, vol. 25, no. 8, pp. 1501–1516, October 2007.

[16] Portland, Oregon, "Official Web site of the City of Portland, Oregon," https://www.portlandoregon.gov, accessed October 30, 201.

[17] J. Khalife, K. Shamaei, and Z. Kassas, "A software-defined receiver architecture for cellular CDMA-based navigation," in *Proceedings of IEEE/ION Position, Location, and Navigation Symposium*, April 2016, pp. 816–826.

[18] Z. Kassas, J. Morales, K. Shamaei, and J. Khalife, "LTE steers UAV," *GPS World Magazine*, vol. 28, no. 4, pp. 18–25, April 2017.